JOURNAL OF MATERIALS SCIENCE 22 (1987) 1535–1546

Effect of processing conditions on physical properties of transition metal–metalloid metallic glasses

A. LOVAS, E. KISDI-KOSZÓ
Central Research Institute for Physics, Budapest, Hungary
L. POTOCKÝ
Faculty of Sciences, P. J. Šafárik University, Košice, Czechoslovakia
L. NOVÁK
Institute of Experimental Physics, Slovak Academy of Sciences, Košice, Czechoslovakia

The influence of processing conditions on the physical properties of transition metal–metalloid based metallic glasses was studied. It was shown that if the melt superheat and cooling rate are changed, the quenched-in stresses and the local environment of the constituent atoms are modified causing remarkable changes in several magnetic, mechanical and chemical properties. In addition, the relaxation characteristics and thermal behaviour were also drastically changed by the processing.

1. Introduction

It is known that several physical properties of crystalline alloys are not only functions of the composition but they also depend sensitively on the whole thermomechanical history of the alloy in question (e.g. effect of cold working, annealing during manufacture). Similarly the properties of nearly perfect single crystals differ from those prepared under less well-controlled conditions.

Such problems can also be found when investigating the physical properties of amorphous alloys following a variation in the technological process. It is plausible that in real amorphous alloys some deviations from the ideally random structure (postulated by modelling) do exist. Such deviations result from quenched-in stresses, topological and chemical inhomogeneities, free volume, phase separation in the amorphous state, clustering, microcrystalline precipitates in the amorphous bulk material or on the surface, etc. It seems that such variations at the atomic and cluster levels – apart from the chemical composition – are strongly influenced by the processing conditions and they modify many physical and chemical properties of the alloy. As a consequence, the physical properties of metallic glass ribbons prepared in the different laboratories exhibit poor reproducibility. Obviously the wide-spread change in properties even at the same composition must be of structural origin; however, there is no quantitative description of this at present. An interesting finding is that variations in processing tend to change these properties often in the same order of magnitude as the change in chemical composition itself.

The aim of this paper is to summarize some of our earlier results in order to show how the processing influences the magnetic, mechanical, electrochemical and thermal properties of transition metal–metalloid (mainly iron-based) glassy alloys prepared by the melt-spinning technique.

2. Background

In the melt-spinning technique (Fig. 1a) the melt jet impinging on the surface of a moving substrate (a rotation wheel) forms a puddle under which a solid layer (ribbon) is formed [1, 2]. The relationship between ribbon thickness and width and the volumetric rate of the melt flow can be obtained from the heat transport-controlled ribbon-formation model [3]. Judging from recent investigations, this model can be regarded as a first approximation. There is evidence that the viscosity of the melt also plays an important role in the geometry of ribbons [4, 5]. At the ribbon–puddle interface a boundary layer of varying viscosity is formed and this also contributes to the formation of the final thickness of the ribbon. Experience has shown that the geometry, as well as the surface morphology and the physical properties, of the ribbon also depend on many other parameters [1, 6–9]. Some of these parameters are given in Table I. Obviously the influence of the given parameters is not independent: the geometry of ribbons, mainly the ratio of their thickness to width, depends on parameters 1 to 7 in Table I; the morphology of the amorphous ribbon (surface roughness, ragged or smooth ribbon edge) is determined by the wheel surface quality, by the atmospheric conditions (vacuum, inert gas, air), and by parameters 8 and 9, etc. From the viewpoint of the resulting physical properties of amorphous ribbons, two processing parameters are of primary importance: the wheel surface velocity and the melt superheat.

The wheel surface velocity strongly influences the cooling rate of the melt. The average cooling rate is

0022–2461/87 $03.00 + .12

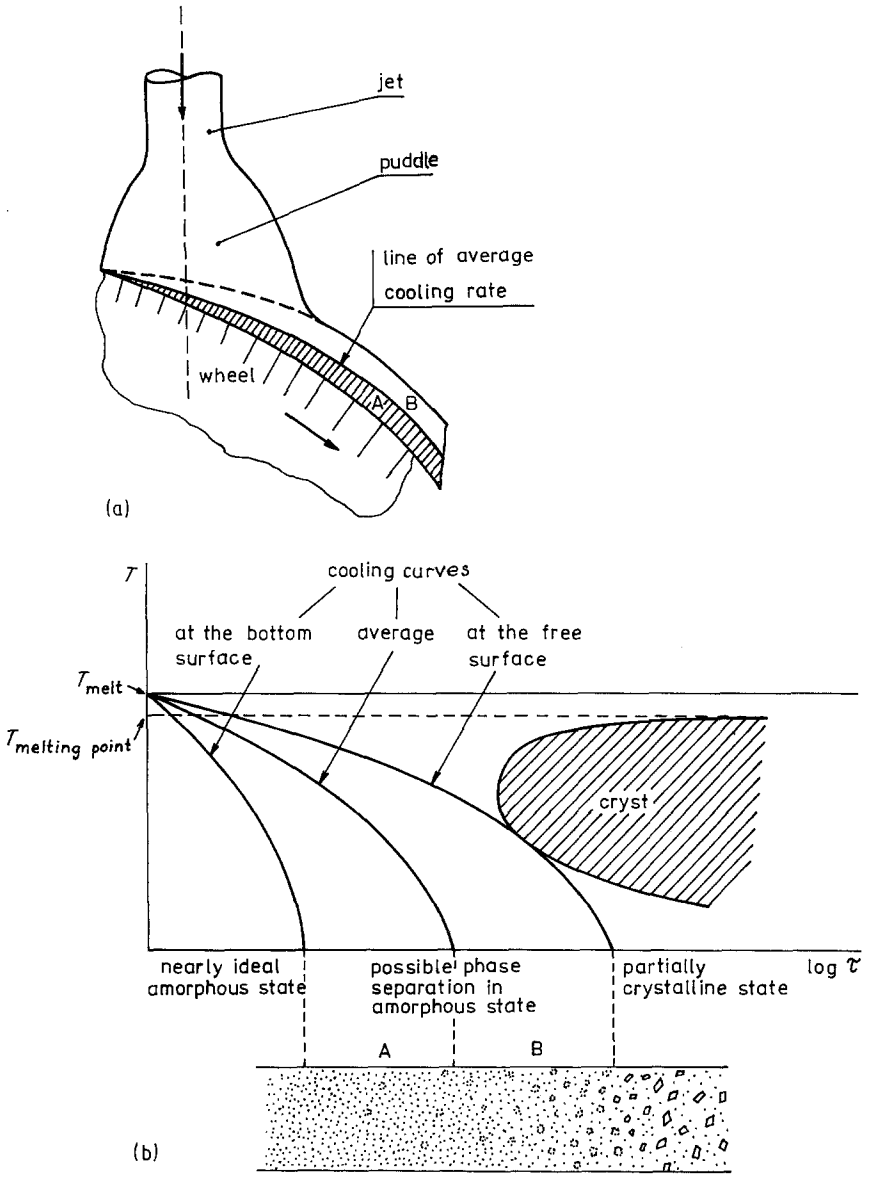

Figure 1 (a) Schematic representation of ribbon formation. (b) Solidification behaviour of the melt during the amorphous ribbon formation; T = temperature, τ = time.

also proportional to the surface velocity. Experience has shown that a higher surface velocity leads to a decrease in ribbon thickness which corresponds to a higher cooling rate. There is a correlation between surface velocity, v, and ribbon thickness, t, as $v = \text{const}/t$ but only for the same alloy composition and melt superheat. Therefore, when comparing different alloys we give the result as a function of ribbon thickness, as this is in direct correspondence with cooling rate, see [6].

The cooling rate varies across the ribbon thickness; therefore, the ribbon cross-section may formally be divided into two regions by the plane representing the average cooling rate of the ribbon (Fig. 1a). In part A (near the wheel) the cooling rate is higher than the average and a good glass-forming condition is fulfilled assuming that the surface of the wheel is smooth enough to prevent heterogeneous nucleation at the ribbon–substrate interface. In contrast, the part near the free surface of the ribbon (part B) can be regarded as being formed under worse glass-forming conditions than at the average cooling rate, but the cooling rate is still high enough to suppress the homogeneous nucleation of the crystalline phases. The appropriate solidification behaviour of the melt is schematically represented in Fig. 1b.

TABLE I Some processing parameters of rapidly quenched ribbons

(1) Melt superheat ($\Delta T = T_{melt} - T_{melting\ point}$)
(2) Ejection pressure
(3) Crucible orifice geometry
(4) Wheel surface velocity (v)
(5) Wheel surface temperature
(6) Puddle length
(7) Contact length
(8) Angle of inclination of crucible
(9) Distance between crucible and wheel

The non-homogeneous cooling conditions may lead to differences in amorphous structures through the cross-section of ribbons. These differences manifest themselves in local changes of stresses and in non-homogeneous distribution of chemical components [10, 11]. In addition, certain surface effects can also be detected, including differences between the wheel side and the free surface [12]. Consequently, the "bulk" physical properties of the amorphous ribbon represent an "average" property which corresponds to an average cooling rate.

The melt superheat also influences the cooling

conditions of the melt: it can indirectly change the structure of the as-quenched alloy. If the temperature of the melt is raised, its viscosity and, consequently, the resulting ribbon thickness decreases. But this does not mean automatically that the average cooling rate will be higher, because the puddle length increases simultaneously. Therefore, the cooling rate is inversely proportional to the ribbon thickness only at constant melt overheat.

Variation of the preparation conditions may result in ribbons having non-identical amorphous structures. Only in some cases do these structures correspond to one of the theoretical models. A series of structure models exists ranging from dense random packing of hard spheres (DRPHS) to "microcrystalline" structure. Some types of mainly metal–metal glasses can be characterized well by the DRPHS model [13]. For transition metal–metalloid glasses, other types of homogeneous but chemically correlated models are more realistic because the covalent bonding character between the constituents is more pronounced [14, 15]. There are theoretical calculations [16] and experimental results [17] which support the existence of intermediate-range order in amorphous alloys.

In the following sections some contributions to the development of the real amorphous structure will be discussed.

3. Discussion

3.1. Quenched-in stresses

Considerable evidence is available to show that during rapid quenching, internal stresses are developed in the ribbon. It may be expected that these quenched-in stresses may be varied by changing the preparation conditions and this can be checked by magnetic and mechanical investigations.

In rapidly quenched amorphous ferromagnetic alloys with non-zero magnetostriction, strain–magnetostriction anisotropy exists as a consequence of the coupling of magnetostriction and internal strains originating from manufacture [18].

In Fe–B amorphous alloys the quenched-in anisotropy (K_q) depends not only on the boron content [19] but the role of the quenching rate can also be detected (Fig. 2) [20]. In this figure the decrease of effective anisotropy (K) as a function of the annealing time (τ_a) is plotted. It is noteworthy that both cooling rates result in higher quenched-in anisotropy at lower boron content. There is evidence that the magnetostriction is strongly affected by the change in procedure. For example for $Fe_{77.6}B_{22.4}$ an increase in the wheel surface velocity by a ratio of 1 : 2 means that the observed magnetostriction falls by about 50% [21]. On applying magnetic annealing the induced anisotropy will again be different for specimens prepared at different cooling rates [20]. This proves that different microstructures are developed during the rapid solidification depending on the preparation conditions. The differences in the microstructure remain in the material even after long-term heat treatments; and the alloys show a "structure memory" effect.

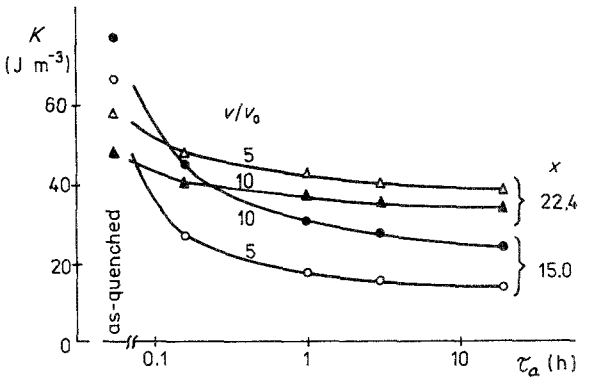

Figure 2 Anisotropy measured after stress-relief annealing as a function of annealing time on ribbons prepared at different cooling rates. v/v_0 is the normalized wheel surface velocity, $v_0 = 5.8\,\mathrm{m\,sec^{-1}}$ [20]. $Fe_{100-x}B_x$, $T_{melt} = 1770\,\mathrm{K}$.

Internal stresses also play an important role in the value of the coercive force in amorphous alloys in view of which it is thought that coercive force is influenced by the processing parameters.

In general, it is accepted that in amorphous alloys large stresses are quenched-in if self-annealing during solidification is suppressed [22]. This can be achieved at very high cooling rates. In this case the coercive force is less sensitive to the applied external stresses [23]. If the cooling rate is lowered the influence of self-annealing will be more and more effective so the coercive force will be smaller. On lowering the quenching rates another effect appears, namely clustering or crystallization, and this leads to an increase in the coercive force. Thus, a minimum coercive force can be achieved using an appropriate cooling rate [6, 24].

This is always the case in binary metal–metalloid ferromagnetic amorphous systems but obviously the composition also plays an important role. In Fig. 3 the thickness-dependence of coercive force is plotted for various Fe–B amorphous alloys. All the individual curves show a minimum whose position depends on boron content. Those minima (as shown by the insert) themselves have a minimum near the eutectic composition. This is in qualitative agreement with the results

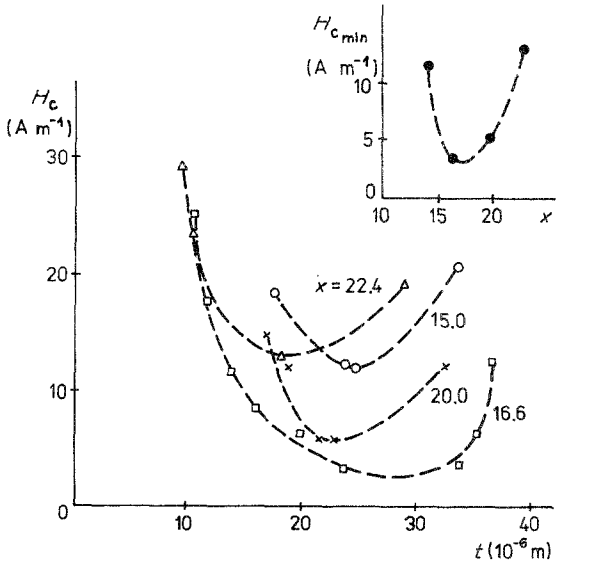

Figure 3 Coercive force plotted against sample thickness. Insert: coercive force minima as a function of boron content. $Fe_{100-x}B_x$, ΔT = constant.

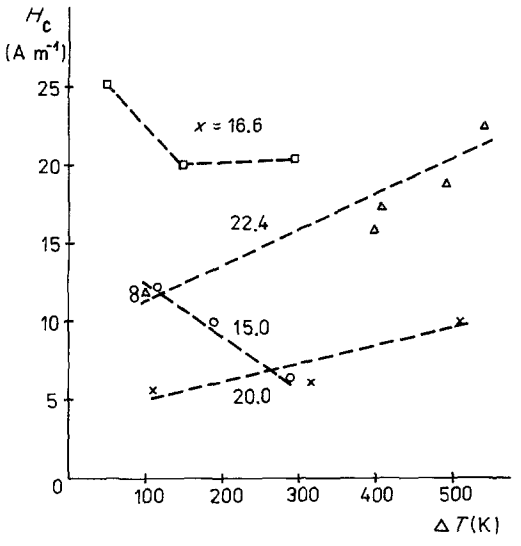

Figure 4 Coercive force as a function of superheat. At every composition the rotation speed was held constant. $Fe_{100-x}B_x$.

of Hagiwara *et al.* [25], where the critical thickness for achieving the amorphous structure was measured. The smallest coercive force value achieved at the eutectic composition is in agreement with earlier results [26]. According to Kisdi-Koszó *et al.* [19] the minimum quenched-in strain magnetostriction anisotropy could be observed near the eutectic composition.

The dependence of coercive force on melt superheat for Fe–B is given in Fig. 4. The observed tendency depends on boron content. Here, at least two competing processes must be taken into account: (1) at higher melt temperatures the viscosity of the melt will be smaller leading to thinner ribbons with higher cooling rate, as has already been mentioned: (2) greater superheat leads to a more homogeneous melt and therefore has, as a consequence, the suppression of phase separation when the ribbons solidify. For the hypoeutectic alloy the coercive force decreases with increasing superheat, for hypereutectic alloys the opposite trend can be found. Hypereutectic alloys have a relatively large tendency to phase separation; therefore, in these alloys the second trend is pronounced. For hypoeutectic alloys the decrease of viscosity with increasing melt superheat seems to be the dominant factor.

Similar to coercive force, quenched-in stresses play an important role in the development of the mechanical properties. If the quenched-in stresses are increased, an increase in tensile strength and in the plasticity of the amorphous alloy can be expected.

The loss of ductility in the heat-treated amorphous alloys (also in the *in situ* heat-treated thicker ribbons) may be the consequence of stress concentrations around clusters and the formation of fracture surfaces [27]. Simultaneously, a change in the nature of chemical bonding also occurs during structural relaxation. As the quenched-in stresses decrease (during relaxation or at lower cooling rates) the bonding state between metal and metalloid atoms increases. A similar explanation may be given when investigating the magnetic after-effect in these alloys. Fig. 5a shows the dependence of tensile strength, Fig. 5b that of bending number on ribbon thickness for two Fe–B alloys (Bending number is a measure of ductility, it gives how many times one can bend the ribbon before it breaks.) In both measured quantities the increase with quenched-in stresses, that is with higher cooling rate, can be seen (in those parts of the cooling rate where H_c increases, see Fig. 3). The microhardness shows an opposite tendency, it increases with decreasing cooling rate (increasing sample thickness, see Fig. 6). This fact can also be understood by taking into account the additional heat treatment of the ribbon during its preparation. This is in qualitative agreement with Köster and Hillenbrand [28]. The dependence of microhardness on the boron content (Fig. 6) is in agreement with Ray *et al.* [29] but the influence of cooling rate may mask this.

In Fig. 7 we see the influence of superheat on microhardness. If the superheat is increased the microhardness decreases. This is explainable by the increasing homogeneity of the melt at higher melt temperatures. As a consequence, the density fluctuation will be lower in the amorphous alloy thereby resulting in a lower stress inside the ribbon. In Figs 8a and b we give the dependence of tensile stress and bending number on the melt superheat. Both quantities increase with increasing superheat thereby demonstrating the significance of homogeneity.

Further proof of the phase separation tendency in Fe–B glasses and the dependence of this feature on processing conditions is given by corrosion resistance investigations [30]. In Fig. 9 the corrosion current is plotted as a function of cooling rate. The curve I_{corr} against v/v_0 shows a drastic change of corrosion current in the range of low cooling rates: this is also a

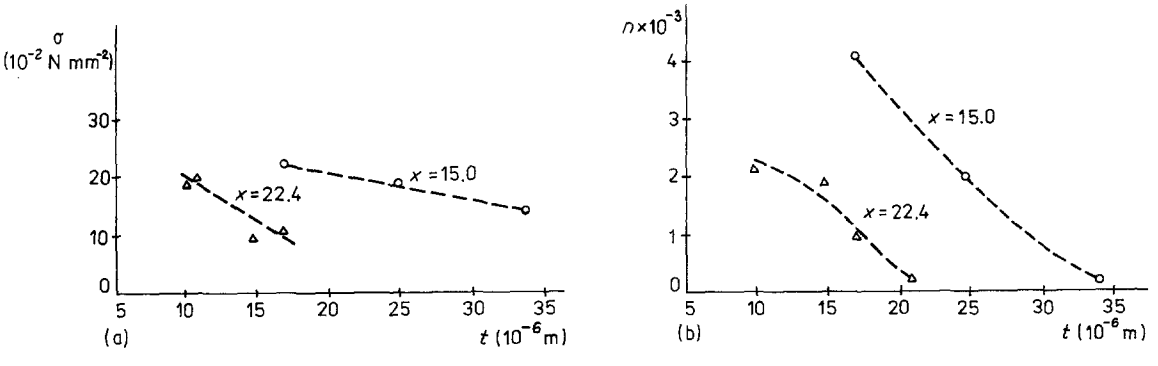

Figure 5 (a) Tensile strength (σ) as a function of sample thickness. (b) Bending number (n) as a function of sample thickness. $Fe_{100-x}B_x$, ΔT = constant.

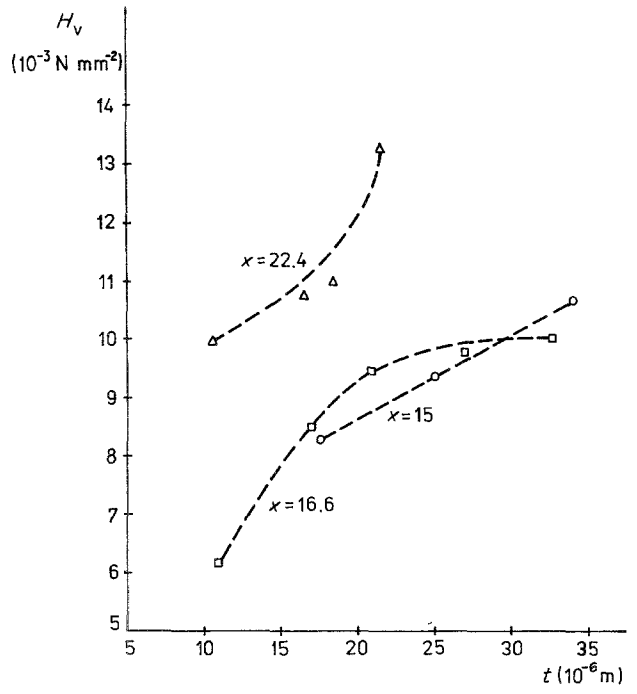

Figure 6 Microhardness plotted against sample thickness. $Fe_{100-x}B_x$, ΔT = constant.

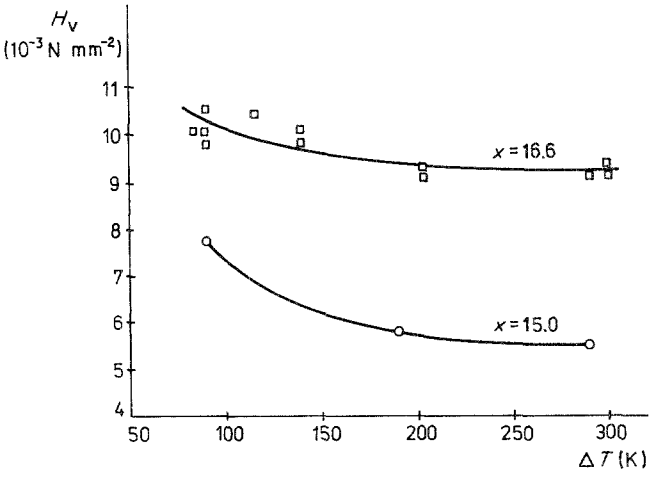

Figure 7 Microhardness as a function of superheat. $Fe_{100-x}B_x$, v/v_0 = constant.

consequence of the increasing phase separation in the slowly cooled glasses. In the region of high cooling rates, I_{corr} slowly increases again due to the increasing stress level. Note that the observed effect of cooling rate on I_{corr} is commensurable with the effect of composition in the case of the binary Fe–B amorphous system. On increasing the boron content from 12 to 22 at %, I_{corr} decreases to one-third of its value (see [30]).

3.2. Chemical short- and intermediate-range order

Evidence shows that many glassy alloys are structurally inhomogeneous [31]. These inhomogeneities may be in the range of nearest neighbour distances; that is, in the short-range order and in the intermediate-range order which is defined for a 2 to 5 nm region. The short-range order may be topological (TSRO) or chemical (CSRO). Probably both can be altered by modifying the processing. In order to detect these alterations, direct experimental investigations are now being carried out in various laboratories and there is already much indirect evidence indicating the change in TSRO and CSRO caused by the processing. A close connection exists between CSRO and Curie temperature (T_c) in ferromagnetic amorphous alloys. The Curie temperature depends on the ferromagnetic exchange between magnetic atoms and thus on the interatomic distances and on the quality of the atoms. Our investigations carried out on some amorphous alloys have verified that the Curie temperature changes with technological parameters [32]. Fig. 10 shows the dependence of Curie temperature on the ribbon thickness (see also [22]). In $Fe_5Co_{50}Ni_{17}Si_{16}B_{12}$ samples, T_c is proportional to the sample thickness. For $Fe_{85}B_{15}$ and $Fe_{39}Ni_{41.6}B_{19.4}$ the opposite tendency was found. It is generally assumed that the increase in T_c with increasing sample thickness can be correlated with additional heat treatment of the ribbon during the rapid solidification, since after any heat treatment the Curie temperature will rise by comparison with the as-quenched state. The same qualitative tendency is caused by partial crystallization as a consequence of the change in chemical composition of the amorphous matrix. The decrease of T_c with increasing sample thickness cannot be interpreted by the mentioned processes. The experimental results suggest that other mechanisms for changing T_c must exist. Our view is that variable frozen-in CSRO exists as a function of processing parameters. The differences in T_c caused by the alteration of processing in some cases remain conserved in the specimens even after long isothermal or after cyclic heat treatments too: this means that there is also a "structural memory" effect, see Fig. 11 [32].

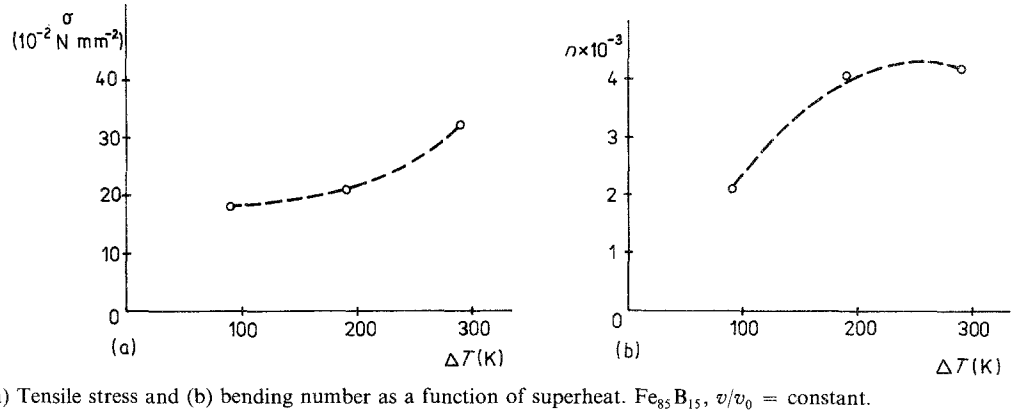

Figure 8 (a) Tensile stress and (b) bending number as a function of superheat. $Fe_{85}B_{15}$, v/v_0 = constant.

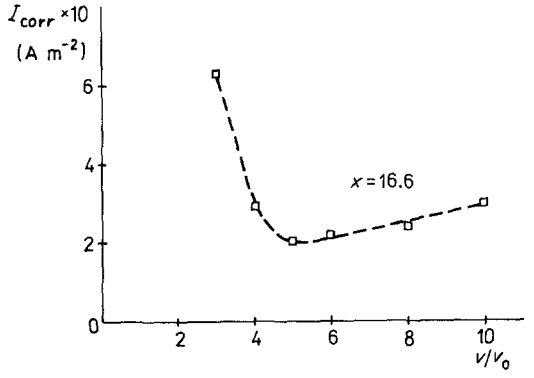

Figure 9 Corrosion current plotted against relative cooling rate [30]. $Fe_{100-x}B_x$.

The inhomogeneities, which act as potential nuclei for the crystallization of amorphous alloys, can also be followed by investigating the kinetics of crystallization (utilizing, for example, the coercive force–temperatures curves). In Fig. 12, such curves can be seen measured on eutectic Fe–B ribbons quenched at different cooling rates [24]. The sudden increase of H_c between 600 and 700 K indicates the onset of crystallization. The initial temperature of crystallization is highest for the ribbons quenched at the highest cooling rate. The maximum on the H_c–T curve is the narrowest for the specimen prepared at the highest cooling rate. This suggests the assumption that the more rapidly cooled specimen is more homogeneous even in the amorphous state. The maximum value of H_c in this temperature range is assumed to be connected with the critical size and distribution of the growing crystalline particles produced by the decomposition of the amorphous matrix. So it can be supposed that the size and distribution of the inhomogeneities in amorphous alloys are also influenced by the cooling rate.

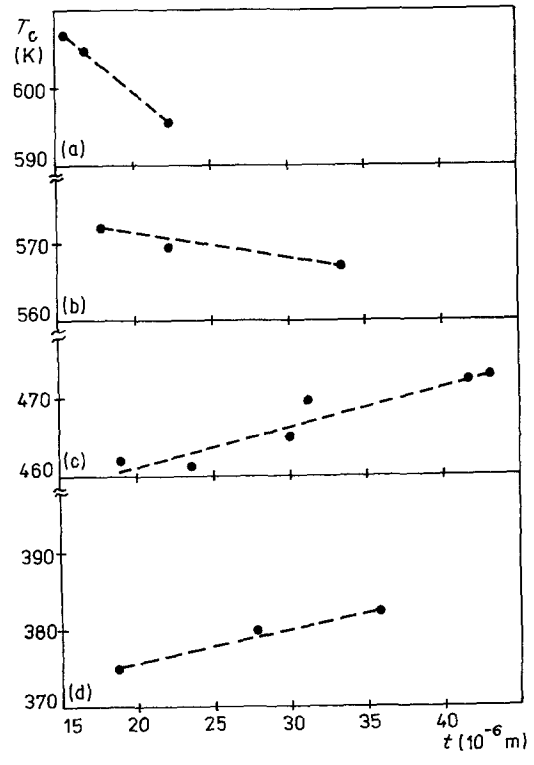

Figure 10 Curie temperature plotted against thickness in (a) $Fe_{39}Ni_{41.6}B_{19.4}$, (b) $Fe_{85}B_{15}$, (c) $Fe_{25}Ni_{55}B_{10}Si_{10}$ and (d) $Fe_5Co_{50}Ni_{17}Si_{16}B_{12}$ [32].

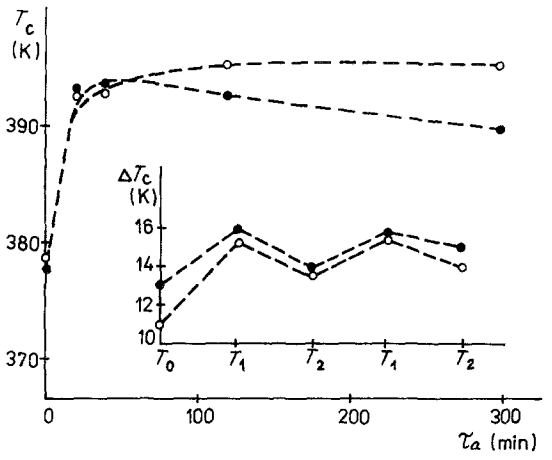

Figure 11 Curie temperature plotted against annealing time (τ_a) in $Fe_5Co_{50}Ni_{17}Si_{16}B_{12}$ prepared at ΔT = 500 K superheat, (□) v = 51 m sec^{-1} and (○) 67 m sec^{-1}, annealed at T_a = 633 K. Insert: change in Curie temperature, ΔT_c, measured from T_c of the as-quenched specimen after cyclic annealings made at T_1 = 633 K for 60 min and at T_2 = 693 K for 30 min [32].

3.3. Free volume

The free volume conception was originally introduced for liquids as the macroscopic excess volume of the liquid compared with the extrapolated volume of the solid [33]. The conception was also extended to amorphous alloys in order to account for the atomic arrangement–rearrangement (structural relaxation). Amorphous alloys have, in general, a slightly lower packing density than a totally close-packed crystalline atomic system. This is caused partly by the steric misfit between the constituent atoms due to their different radii and partly by the non-equilibrium chemical bonding state in random arrangement. It has been pointed out that the microscopic free volume in amorphous alloys consists of vacancy-like and of extended defects as a result of density fluctuations between low- and high-density regions. The low-density regions can be regarded as free volume-like, the high-density regions as anti-free volume-like. The consequence of the density fluctuations is the presence of long-, medium- and atomic-scale internal stresses in the amorphous alloys [34].

The free volume can be investigated by several methods. A decrease in the macroscopic free volume due to structural relaxation was detected by density measurements [35]. From the microscopic point of view, positron annihilation is able to give information about the presence and the type of free volume. The free volume may act as low electron density sites, which are trapping centres for positrons. It is therefore plausible that if the free volume and vacancy-like defects can be modified by the processing, a corresponding change in positronium lifetime can be detected. In Figs 13 to 15 the results of positron annihilation investigations on amorphous $Fe_{40}Ni_{40}Si_{14}B_6$ alloys are summarized [36]. The dependence of positron lifetimes, τ_1 and τ_2, and relative intensity, I_2, are plotted in Fig. 13 as a function of ribbon thickness and surface velocity. The increase of τ_1 and τ_2 values with

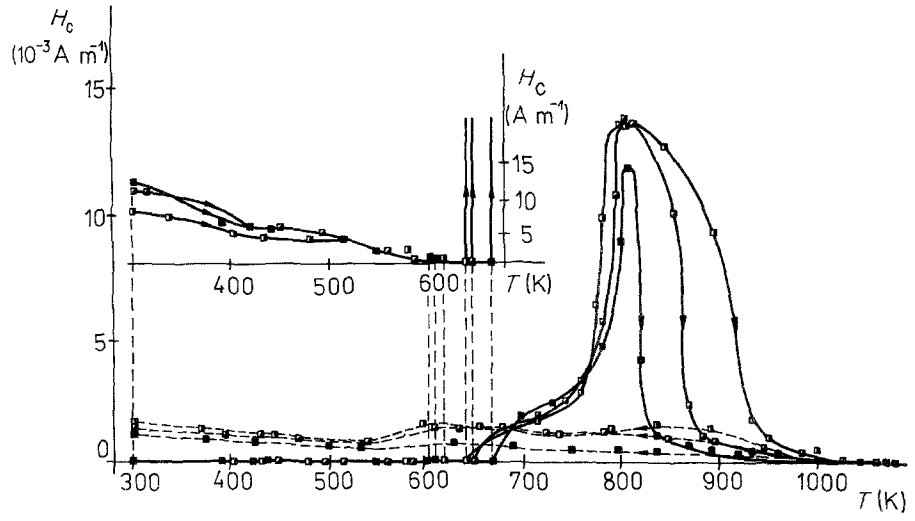

Figure 12 Coercive force against temperature curves measured on eutectic Fe–B ribbons quenched at different cooling rates [24]. $Fe_{83.4}B_{16.6}$, (■) 8073 rev min^{-1}, v/v_0 = 6.5; (▨) 8694 rev min^{-1}, v/v_0 = 7.0; (■) 12 420 rev min^{-1}, v/v_0 = 10.0.

increasing cooling rate indicates an increase in the size of the vacancy-like trapping centres, thus suggesting that a higher cooling rate results in greater free volume. The appearance of the much longer lifetime τ_2 indicates that some agglomeration of free volume-like defects also exists; however, its relative intensity, I_2, is small and decreases with lower cooling rates. The influence of melt superheat on the quenched-in free volume was also investigated by positron annihilation (Fig. 14); the variation of melt superheat only slightly changes the free volume. Fig. 15 shows that the effect of structural relaxation on the change of free volume can also be detected. From Fig. 15 it is clear that the positron lifetime decreases as the vacancy-like free volume anneals out. At higher temperatures the lifetime again increases, possibly as a consequence of clustering before crystallization.

There is also a connection between the free volume and the magnetic after-effect. According to Kronmüller and Moser [37] the magnetic after-effect in amorphous alloys has a two-fold origin: one arises from the atom pair reorientation similar to that found in crystalline alloys. It is assumed that the mechanism of the atom pair reorientation process in a "two-level system" is similar to Anderson's model [38] developed to describe excitations in glasses. The second one is the Snoek-type magnetic relaxation of metalloid atoms. In Snoek-type relaxation the jump of metalloid atoms between "interstitial" sites is involved. In binary metal–metalloid glasses (Fe–B, Co–B), the after-effect may be of Snoek-type origin. Obviously not all metalloid atoms cause magnetic relaxation; the contribution of metalloid atoms to the relaxation depends on the local environment and on the bonding state of the metalloid atom. In the free volume–antifree volume conception it can be imagined that stronger and weaker bonding states between the metal–metalloid atoms may exist in the amorphous matrix. Distribution of these regions may vary with changing cooling rate. This feature is supported by the magnetic after-effect measurements on $Fe_{83}B_{17}$ ribbons, see Fig. 16 [39]. Here one can see that on increasing the cooling rate, the magnetic after-effect also increases. In Fig. 17 a similar dependence is plotted for $Fe_{100-x}B_x$ (x = 15 and 22.4 at %) alloys in the as-quenched state as well as after annealing. Structural relaxation led to a significant decrease of the after-effect as illustrated by the figure. This is the consequence of annealing out of the vacancy-like free volume and the increasing bonding state of boron atoms. It is interesting that samples produced by different cooling rates show differences in magnetic after-effect even after the heat treatment.

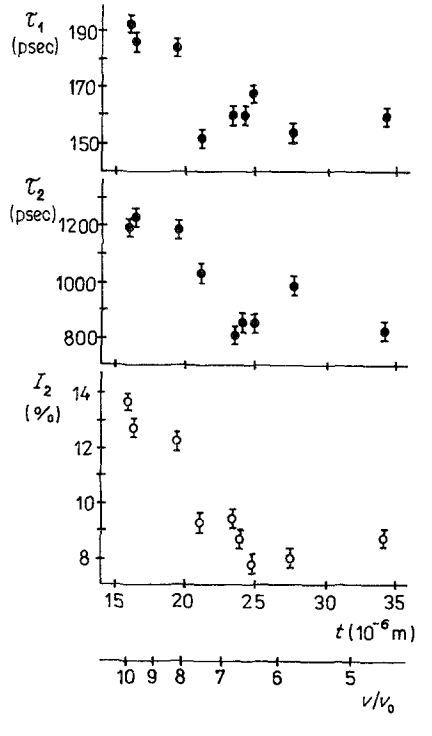

Figure 13 Positron life-time and relative intensity plotted against sample thickness and normalized surface velocity; v_0 = 5.8 m sec^{-1} [36]. $Fe_{40}Ni_{40}Si_{14}B_6$.

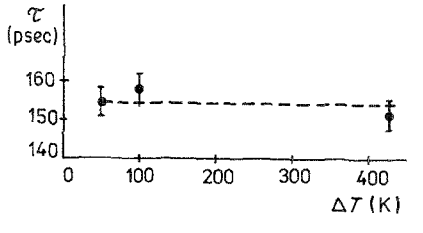

Figure 14 Positron life-time plotted against melt superheat [36]. $Fe_{40}Ni_{40}Si_{14}B_6$, v/v_0 = 3.

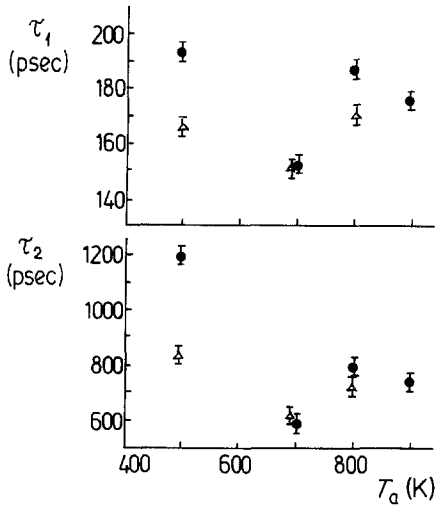

Figure 15 Positron life-time plotted against isochron heat-treatment temperatures. The time duration of heat treatments was always 2 h [36]. $Fe_{40}Ni_{40}Si_{14}B_6$. (○) $v/v_0 = 3$; (△) $v/v_0 = 10$.

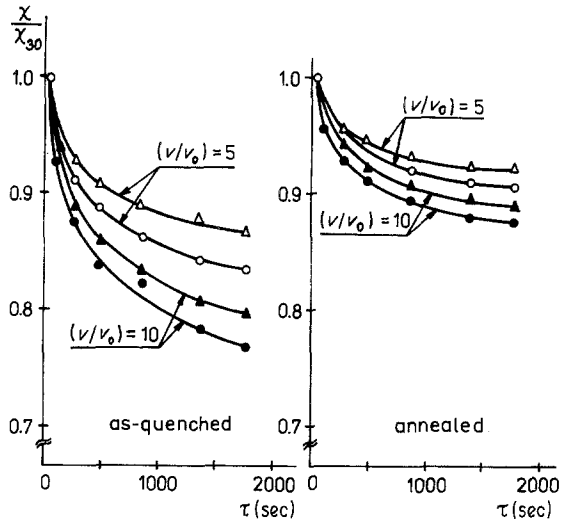

Figure 17 Time decrease of relative initial susceptibility in (○, ●) $Fe_{85}B_{15}$ and (△, ▲) $Fe_{77.6}B_{22.4}$ amorphous alloys in as-quenched and annealed state [39].

3.4. Thermal stability and crystallization kinetics

Between various as-quenched amorphous ribbons differences can be found in the degree of self-annealing taking place during the rapid solidification. If the cooling rate is sufficiently slow some kind of "structural relaxation" occurs during the quenching process itself. This is reflected by many physical properties, e.g. by the lowering of the coercive force (see Fig. 3). A consequence of the self-annealing is that the appropriate relaxation energy changes. Typical heat-release curves are given in Fig. 18. The differences can be seen between the thin and thick samples in the course of the relaxation process. Thick ribbons are already partially relaxed in the as-quenched state so the relaxation energy decreases as the ribbon thickness increases (see Fig. 19) [22].

Self-annealing also alters the character of the phase-separation tendency and may, therefore, influence the crystallization kinetics and the thermal stability of the alloy. If one investigates the kinetics of the amorphous–crystalline transition the dependence of kinetic parameters on the preparation conditions can be found [40]. As an example, the eutectic Fe–B alloy was studied by the DSC method. Kinetic parameters are listed in Table II.

The results show that the kinetic parameters are practically independent of the heating rate for slowly quenched ribbons. This suggests that here the crystallization mainly takes place with the growth of quenched-in nuclei. Because the Avrami exponent (n) for the sample prepared at high cooling rate is significantly higher and shows a marked dependence on the heating rate, the nucleation process in the crystallization obviously plays a decisive role. An example of the influence of cooling rate on the thermal stability of the Fe–B system is seen in Figs 20 and 21. For the eutectic and hypereutectic regions the onset of crystallization is shifted to higher temperatures and the amorphous–crystalline transition will be sharper as the cooling rate increases. Fig. 22 gives the thermomagnetic curves of $Fe_{83.4}B_{16.6}$ prepared at two different cooling rates. With a higher cooling rate the crystallization process is characterized by a narrower curve. This suggests that the more rapidly cooled samples crystallize as more homogeneous. This is also supported by the coercive force investigations (Fig. 12). With regard to the crystallization of hypoeutectic Fe–B alloys, Fig. 23 demonstrates that the crystallization is

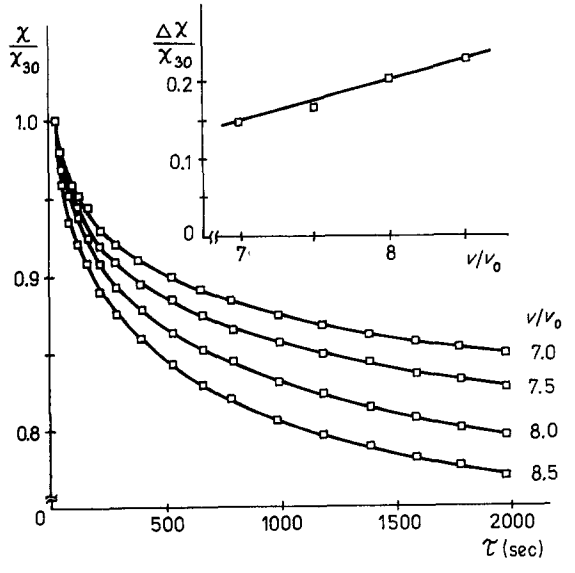

Figure 16 Time decrease of initial susceptibility after demagnetization on as-quenched $Fe_{83.5}B_{16.5}$ samples prepared at various cooling rates. Insert: magnetic after-effect, $\Delta\chi/\chi_{30}$ as a function of the relative cooling rate [39].

TABLE II Kinetic parameters of the crystallization of eutectic Fe–B [40].

Heating rate ($K\,min^{-1}$)	$v/v_0 = 3$		$v/v_0 = 10$	
	k_0 $10^{17}\,sec^{-1}$	n	k_0 $10^{19}\,sec^{-1}$	n
2.5	1.5	2.2 ± 0.15	2.0	4.2 ± 0.4
5	1.75	2.0 ± 0.1	2.4	6.5 ± 0.3
10	1.5	1.8 ± 0.1	3.0	13 ± 2
20	1.7	2.2 ± 0.1	3.9	16 ± 5
Crystallization energy	254 ± 4 kJ mol^{-1}		290 ± 20 kJ mol^{-1}	

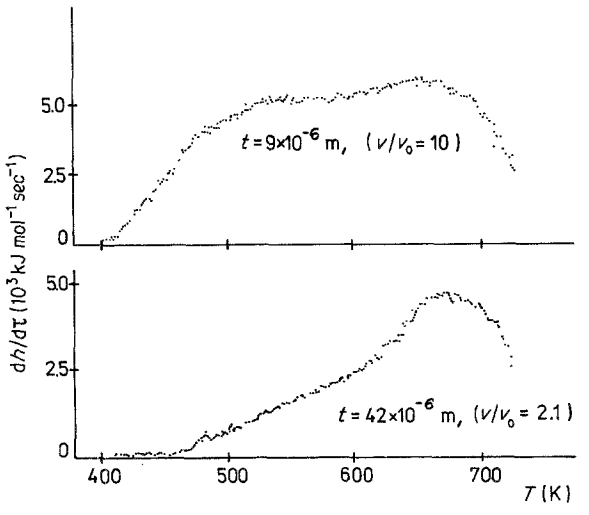

Figure 18 Typical heat release curves: in $t = 9 \times 10^{-6}$ m and $t = 42 \times 10^{-6}$ m thick ribbons prepared with $v/v_0 = 10$ and 2.1, $v_0 = 5.8$ m sec^{-1} surface velocity [22]. $Fe_{25}Ni_{55}Si_{10}B_{10}$.

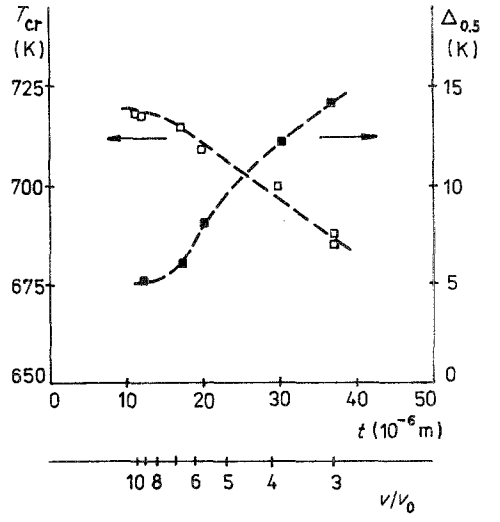

Figure 20 Crystallization temperature, T_{cr}, and half-width of crystallization peak ($\Delta_{0.5}$) plotted against sample thickness and normalized surface velocity for $Fe_{83.4}B_{16.6}$; $v_0 = 5.8$ m sec^{-1} [40].

separated into two stages [41]. In this figure the thermogram is given for rapidly and slowly cooled $Fe_{85}B_{15}$ alloy. The influence of the cooling rate is obvious. The higher cooling rate leads to a more pronounced separation of the two peaks showing that α-Fe precipitation takes place earlier in the alloy prepared at a higher cooling rate. On the other hand, the crystallization of Fe_3B shifted to the higher temperature. The influence of cooling rate may be interpreted by supposing a phase separation tendency exists in this amorphous system. In the hypoeutectic Fe–B glasses the decomposition into iron-rich and boron-rich clusters may be assumed to depend on the processing.

4. Influence of amorphous ribbon processing on the properties of inductive elements used as magnetic devices

In the previous sections, the role of fabrication conditions on a wide range of physical properties has been demonstrated. It was emphasized that the modification in cooling rate leads to a change in the "frozen-in" structure. It was also pointed out that the differences in several magnetic properties such as magnetic after-effect and quenched-in anisotropy developed during the quenching process cannot be completely removed by heat treatments.

The influence of ribbon-processing on the properties of toroids directly utilized as soft magnetic devices is rarely treated in the literature. Some of the device-oriented applications, like moving coil transformers [42] or filters (especially in current-compensated modes), require high initial permeability [43] which is only attainable using suitable heat treatment. It is, therefore, important to know how the quenched-in thermal history of ribbons manifests itself during the subsequent heat treatments carried out in wound form in the initial permeability (μ_i) attainable [44].

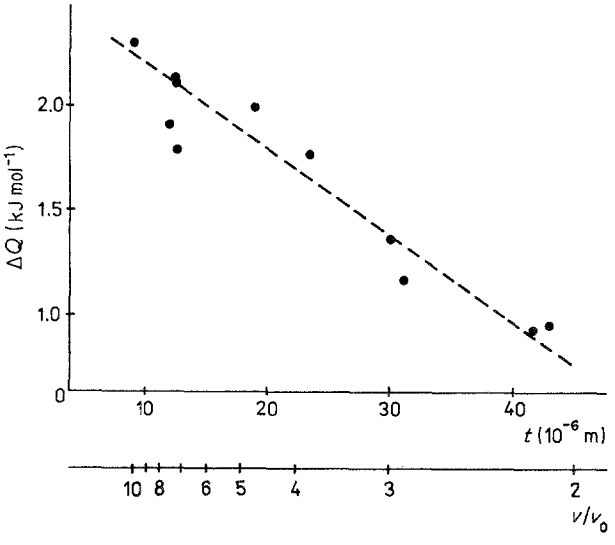

Figure 19 Relaxation energy plotted against thickness and normalized surface velocity, $v_0 = 5.8$ m sec^{-1} [22]. $Fe_{25}Ni_{55}Si_{10}B_{10}$.

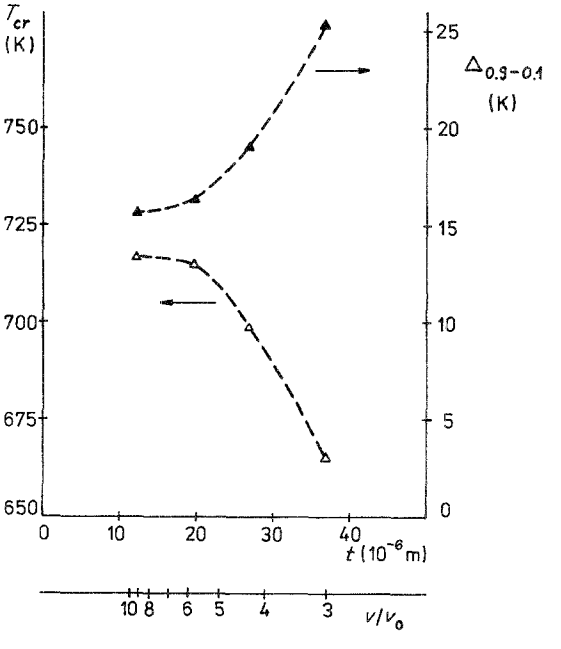

Figure 21 Crystallization temperature, T_{cr}, and width of crystallization peak plotted against sample thickness and normalized surface velocity for $Fe_{77.6}B_{22.4}$. The width of crystallization peak ($\Delta_{0.9-0.1}$) denotes the temperature difference between the 10% and 90% crystallized sample, $v_0 = 5.8$ m sec^{-1}.

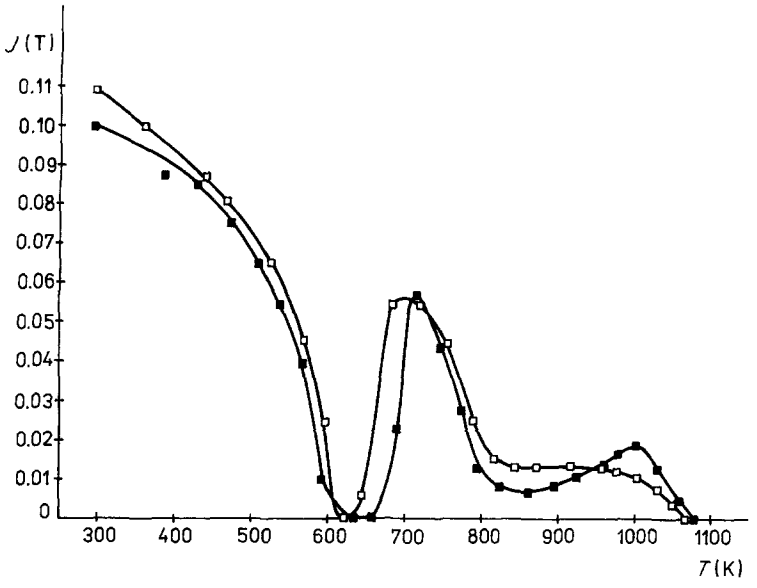

Figure 22 Thermomagnetic curves of $Fe_{83.4}B_{16.6}$ ribbons prepared at different cooling rates. T_{melt} = 1570 K, (□) 3726 rev min^{-1}, (■) 12'420 rev min^{-1}.

For this purpose a series of $Fe_{80}Si_6B_{13}C_1$ and $Fe_{6.4}Ni_{16.2}Co_{51.6}Cr_{4.0}Si_{7.6}B_{14.3}$ (having high and nearly zero magnetostriction, respectively) amorphous ribbons were prepared at different cooling rates. Subsequently, they were wound in the form of toroids with an outer diameter of 22 mm. μ_i as well as H_c were measured on toroids and on straight ribbons after the rapid quenching and after isothermal heat treatment at temperatures between 350 and 430° C.

4.1. Toroids

The influence of isothermal heat treatments on the initial permeability of $Fe_{80}Si_6B_{13}C_1$ toroids is presented in Fig. 24. In spite of the significant difference in ribbon thickness (on the thickest ribbon, traces of surface crystallinity could be detected), the measured permeabilities in the as-quenched state were similar. The permeability of thick and thin ribbons shows an increasing difference with the time of annealing at 350° C even after 500 min. The μ_i of the thick ribbons is always lower than that of the thin ones at any annealing time. Annealing carried out at higher temperatures results in higher values of μ_i. This indicates that the structural ordering responsible for reaching the optimum value of permeability is not completed even after the 120 min annealing at 380° C. The difference in the quenched-in structure is conserved in the ribbons during the heat treatments up to the beginning of crystallization when the permeability drops again. The coercive force on the toroids was also measured to monitor stress relaxation, see Fig. 25. It is noteworthy that both the stress relaxation and the structural ordering which led to high permeability and also the subsequent crystallization take place earlier in the thinner ribbon.

Similar results were obtained on $Fe_{6.4}Co_{51.6}Ni_{16.1}$-$Cr_{4.0}Si_{7.6}B_{14.3}$ toroids but the difference between the thick and thin ribbons seems to disappear at 415° C.

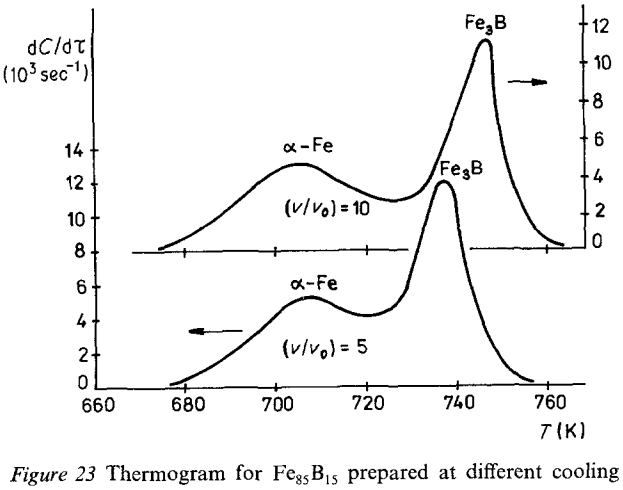

Figure 23 Thermogram for $Fe_{85}B_{15}$ prepared at different cooling rates.

4.2. Straight ribbons

Because of the magneto-mechanical coupling, the heat treatment of a toroid means a treatment under stress. In order to separate this effect, experiments were also carried out on straight ribbons. The result for the $Fe_{80}Si_6B_{13}C_1$ alloy are given in Fig. 26, where the $\mu_i/\mu_{i\,asq}$ values are plotted as a function of the annealing time. The other alloy behaves similarly. It is obvious that all of the heat treatments used result in different μ_i depending on the cooling rate applied during quenching. The differences between the straight samples are more pronounced than those obtained on toroids.

The thickness-dependent saturation values suggest that the inherent structural state determined by the applied quenching rate in the sample survives even after intensive heat treatments. Heat treatment of a toroid, where stress relaxation is combined with the development of stress-induced anisotropy, seems to promote a decrease of the above "memory effect" developing during the quenching process.

5. Conclusions

Similar to the crystalline alloys, the conditions of preparation also play a decisive role in the development of the physical properties of melt-spun glassy alloys. The sensitive processing-dependence of macroscopic physical properties is based on the existence of "real structure" which is often different from that of "ideal" – described by the modelling. Real structures can be characterized by the quenched-in stresses,

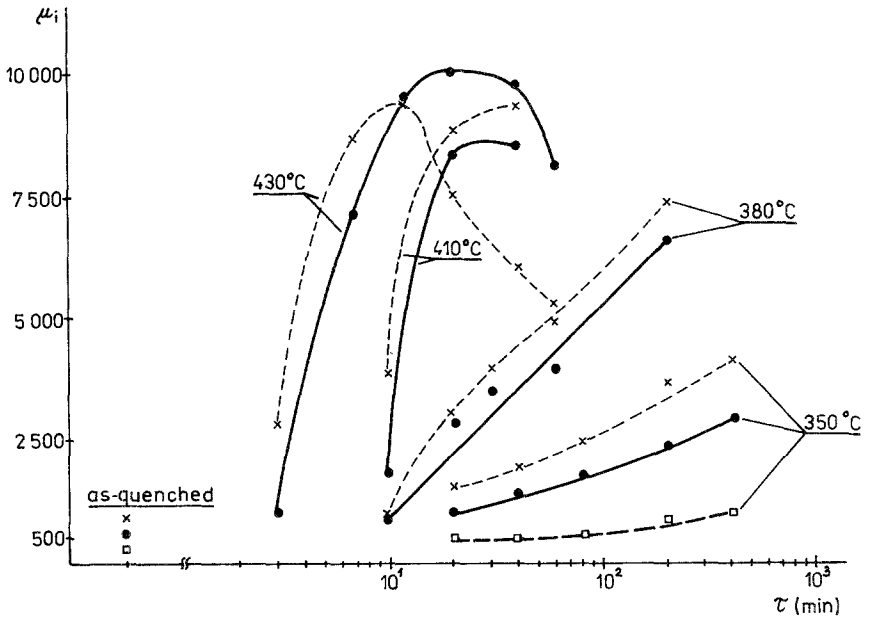

Figure 24 Initial permeability of toroids plotted against annealing time during isothermal heat treatments made at different temperatures for different ribbon thickness [44]. $Fe_{80}Si_6C_1B_{13}$; (x) 30 μm, (●) 45 μm, (□) 55 μm.

micro-inhomogeneities in the scale of short- and intermediate-range order, microcrystalline precipitates on the surfaces, etc. The observed changes in the physical properties have been proposed as being linked with structural phenomena such as stresses, the change in short- and intermediate-range order, and the phase-separation in the amorphous state.

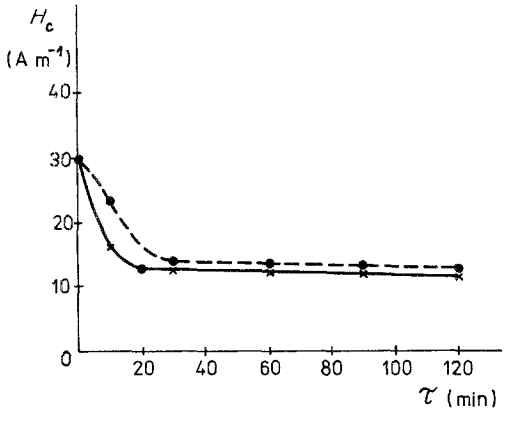

Figure 25 Coercive force of $Fe_{80}Si_6B_{13}C_1$ toroids plotted against annealing time for different ribbon thicknesses [44]. T_a = 380° C; (x) 30 μm, (●) 45 μm.

1. The alteration of quenched-in stresses manifests itself as a change in quenched-in magneto-elastic anisotropy. This is reflected mainly in H_c, which plays an important role in the optimization of soft magnetic properties. Varying quenched-in stresses are also well reflected in the mechanical properties of ribbons such as tensile strength, ductility and microhardness.

2. The frozen-in short- and intermediate-range order can also be modified by the processing which alters the ferromagnetic exchange. This modified order remains conserved even after long isothermal heat treatments (structural memory effect).

3. The sensitivity of structure on processing is also reflected in the distribution of free volume (positron annihilation).

4. It was also found that the thermal behaviour (heat release, temperature and kinetics of crystallization) is modified by the applied cooling rate.

5. Stress-induced anisotropy developing during heat treatments in toroid form decreases the effect of the quenched-in structure on the response to heat treatments.

Acknowledgements

We gratefully acknowledge the discussions with Drs

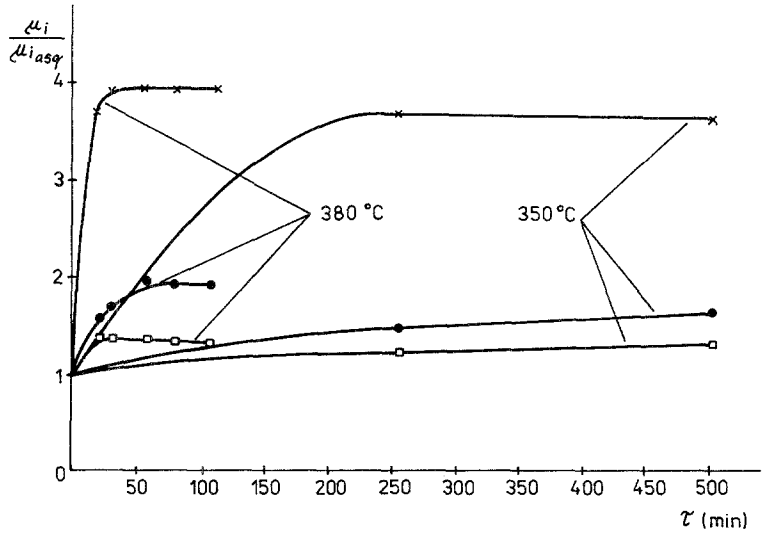

Figure 26 As Fig. 24, but for straight ribbons [44].

L. Gránásy, P. Vojtaník and Zs. Kajcsos, and the measured data placed at our disposal by them. We are very grateful to Dr G. Konczos for his careful reading of the manuscript and for his valuable remarks.

References

1. H. H. LIEBERMANN and C. D. GRAHAM, *IEEE Trans. Magn.* **MAG-12** (1976) 921.
2. H. HILLMANN and H. R. HILZINGER, in "Rapidly Quenched Metals", Vol. III, edited by B. Cantor (The Metals Society, London, 1978) p. 22.
3. S. KAVESH, in "Metallic Glasses", edited by J. J. Gilman and H. J. Leamy (American Society for Metals, Metals Park, Ohio, 1976) p. 36.
4. P. den DECKER and A. DREVERS, in "Proceedings of the International Conference on Metallic Glasses; Science and Technology", Vol. I, edited by C. Hargitai, I. Balconyi and T. Kemèny (Distributor Kultura, Budapest POB 49, 1981) p. 181.
5. L.GRÁNÁSY, Thesis, R. Eötvös University, Budapest (1981).
6. F. E. LUBORSKY, H. H. LIEBERMANN and J. L. WALTER, in "Proceedings of the International Conference on Metallic Glasses; Science and Technology", Vol. I, edited by C. Hargitai, I. Balconyi and T. Kemèny (Distributor Kultura, Budapest POB 49, 1981) p. 203.
7. F. E. LUBORSKY, SHYH-CHIN HUANG and H. C. FIEDLER, *IEEE Trans. Magn.* **MAG-17** (1981) 3463.
8. H. FIEDLER, H. MÜHLBACH and G. STEPHANI, *J. Mater. Sci.* **19** (1984) 3229.
9. C. KOPASZ, B. MOLNÁR, G. MÁRKI, B. ALBERT, C. HARGITAI and G. SZOLCSÁNYI, *J. Magn. Magn. Mater.* **41** (1984) 93.
10. Á. Z. NAGY, B. VASVÁRI, P. DUWEZ, L. BAKOS, J. BOGÁNCS and V. M. NAZAROV, *Phys. Status Solidi (a)* **61** (1980) 689.
11. I. NAGY, T. TARNÓCZI, M. HOSSÓ and F. PAVLYÁK, in "Proceedings of the International Conference on Metallic Glasses; Science and Technology", Vol. I, edited by C. Hargitai, I. Balconyi and T. Kemèny (Distributor Kultura, Budapest POB 49, 1981) p. 223.
12. É. KISDI-KOSZÓ, L. POTOCKÝ, P. KOLLÁR, Z. JURANEK and G. VÉRTESY, in Proceedings of Soft Magnetic Materials 7 Conference, Blackpool (1985), (Wolfson Centre, Cardiff, 1986) p. 335.
13. F. SPAEPEN and G. S. CARGILL III, in "Rapidly Quenched Metals", edited by S. Steeb and H. Warlimont (Elsevier, Amsterdam, 1985) p. 581.
14. D. S. BOUDREAUX, in "Glassy Metals: Magnetic, Chemical and Structural Properties", edited by R. Hasegawa (CRC, Florida, 1983) p. 1.
15. I. VINCZE, T. KEMÉNY, A. S. SCHAAFSMA, A. LOVAS and F. van der WOUDE, in "Proceedings of the International Conference on Metallic Glasses; Science and Technology", Vol. I, edited by C. Hargitai, I. Balconyi and T. Kemèny (Distributor Kultra, Budapest POB 49, 1981) p. 361.
16. P. H. GASKELL, in "Rapidly Quenched Metals", edited by S. Steeb and H. Warlimont (Elsevier, 1985) p. 413.
17 P. H. GASKELL, L. A. FREEMAN and D. J. SMITH, in "Proceedings 4th Conference on Rapidly Quenched Metals", Vol. I, Sendai 1981, edited by T. Masumoto and K. Suzuki (The Japan Institute of Metals, Sendai, 1982) p. 439.
18. R. C. O'HANDLEY, in "Amorphous Metallic Alloys", edited by F. E. Luborsky (Butterworths Monographs in Materials, 1983) p. 272.
19. É. KISDI-KOSZÓ, L. POTOCKÝ and L. NOVÁK, *J. Magn. Magn. Mater.* **15-18** (1980) 1383.
20. L. NOVÁK, É. KISDI-KOSZÓ, L. POTOCKÝ and A. LOVAS, in "Proceedings of the International Conference on Metallic Glasses; Science and Technology", edited by C. Hargitai, I. Balconyi and T. Kemèny (Distributor Kultura, Budapest POB 49, 1981) p. 229.
21. L. POTOCKÝ, R. MLÝNEK, É. KISDI-KOSZÓ, J. TAKÁCS and P. SAMUELY, in "Proceedings of the International Conference on Metallic Glasses; Science and Technology", Vol. I, edited by C. Hargitai, I. Balconyi and T. Kemèny (Distributor Kultura, Budapest POB 49, 1981) p. 101.
22. L. GRÁNÁSY and A. LOVAS, *J. Magn. Magn. Mater.* **41** (1984) 113.
23. R. GRÖSSINGER, H. SASSIK and A. LOVAS, *ibid.* **41** (1984) 107.
24. L. NOVÁK, L. POTOCKÝ, A. LOVAS, É. KISDI-KOSZÓ and J. TAKÁCS, *ibid.* **19** (1980) 149.
25. M. HAGIWARA, A. INOUE and T. MASUMOTO, *Sci. Rep. Ritu* **29** (1981) 351.
26. C. HARGITAI and A. LOVAS, in "Proceedings of the Soft Magnetic Materials 3 Conference", edited by O. Benda, I. Mayer and J. Sláma, Part 2, (Vytalčilo Edičné stredisko SVŠT, Bratislava, 1978) p. 564.
27. H. S. CHEN, *Rep. Prog. Phys.* **43** (1980) 353.
28. U. KÖSTER and H. G. HILLENBRAND, in "Proceedings of the International Conference on Metallic Glasses; Science and Technology", Vol. I, edited by C. Hargitai, I. Balconyi and T. Kemèny (Distributor Kultura, Budapest POB 49, 1981) p. 91.
29. R. RAY, R. HASEGAWA, C. P. CHOU and L. A. DAVIS, *Scripta Metall.* **11** (1977) 973.
30. J. FARKAS, in "Proceedings of the International Conference on Metallic Glasses; Science and Technology", Vol. II, edited by C. Hargitai, I. Balconyi and T. Kemèny (Distributors Kultura, Budapest POB 49, 1981) p. 367.
31. J. DURAND, "Magnetism in transition metal base amorphous alloys", in "Glassy metals: magnetic, chemical and structural properties", edited by R. Hasegawa (CRC, Florida, 1983) p. 147.
32. A. LOVAS, L. POTOCKÝ, L. NOVÁK and É. KISDI-KOSZÓ, *IEEE Trans. Magn.* **MAG-17** (1981) 2712.
33. M. H. COHEN and D. TURNBULL, *J. Chem. Phys.* **31** (1959) 1164.
34. T. EGAMI, *IEEE Trans. Magn.* **MAG-17** (1981) 2600.
35. B. TOLONI, A. KURSUMOVIC and R. W. CAHN, *Scripta Metall.* **19** (1985) 947.
36. Zs. KAJCSOS, L. MARCZIS, A. LOVAS, É. KISDI-KOSZÓ, D. KISS, Cs. SZELES and G. BRAUER, *Nucl. Instrum. Methods* **199** (1982) 327.
37. H. KRONMÜLLER and N. MOSER, in "Amorphous Metallic Alloys", edited by F. E. Luborsky (Butterworths Monographs in Materials, London, 1983) p. 341.
38. F. W. ANDERSON, "Lectures on Amorphous Systems", in "Physics of Ill-Condensed Matter", edited by R. Bolian, R. Maynard and G. Toulouse (North Holland, Amsterdam, 1979).
39. P. VOJTANÍK, É. KISDI-KOSZÓ, A. LOVAS and L. POTOCKÝ, in "Proceedings of the International Conference on Metallic Glasses; Science and Technology", Vol. I, edited by C. Hargitai, I. Balconyi and T. Kemèny (Distributor Kultura, Budapest POB 49, 1981) p. 247.
40. L. GRÁNÁSY, A. LOVAS and T. KEMÉNY, *ibid.*, p. 197.
41. T. KEMÉNY, I. VINCZE, B. FOGARASSY and S. ARAJS, *Phys. Rev.* **B20** (1979) 476.
42. J. SZÖLLÖSY, A. LOVAS, L. VARGA and G. KONCZOS, Hungarian Patent 4227/83 (1983).
43. F. E. LUBORSKY, in "Amorphous metallic alloys", edited by F. E. Luborsky (Butterworths Monographs in Materials, London, 1983) p. 360.
44. A. LOVAS, L. F. KISS, G. KONCZOS and A. SOLYOM, in Proceedings of the Soft Magnetic Materials 7 Conference, Blackpool (1985), (Wolfson Centre, Cardiff, 1986) p. 321.

Received 27 March
and accepted 5 August 1986